The Plant Cell, Vol. 24: 4539–4554, November 2012, www.plantcell.org

FIMBRIN1 Is Involved in Lily Pollen Tube Growth by Stabilizing the Actin Fringe[C][W][OA]

Hui Su, Jinsheng Zhu, Chao Cai, Weike Pei, Jiaojiao Wang, Huaijian Dong, and Haiyun Ren[1]

Key Laboratory of Cell Proliferation and Regulation Biology of Ministry of Education, College of Life Science, Beijing Normal University, Beijing 100875, People's Republic of China

An actin fringe structure in the subapex plays an important role in pollen tube tip growth. However, the precise mechanism by which the actin fringe is generated and maintained remains largely unknown. Here, we cloned a 2606-bp full-length cDNA encoding a deduced 77-kD fimbrin-like protein from lily (*Lilium longiflorum*), named FIMBRIN1 (FIM1). Ll-FIM1 was preferentially expressed in pollen and concentrated at actin fringe in the subapical region, as well as in longitudinal actin-filament bundles in the shank of pollen tubes. Microinjection of Ll-FIM1 antibody into lily pollen tubes inhibited tip growth and disrupted the actin fringe. Furthermore, we verified the function of Ll-FIM1 in the *fim5* mutant of its closest relative, *Arabidopsis thaliana*. Pollen tubes of *fim5* mutants grew with a larger diameter in early stages but could recover into normal forms in later stages, despite significantly slower growth rates. The actin fringe of the *fim5* mutants, however, was impaired during both early and late stages. Impressively, stable expression of *fim5pro:GFP:Ll-FIM1* rescued the actin fringe and the growth rate of *Arabidopsis fim5* pollen tubes. In vitro biochemical analysis showed that Ll-FIM1 could bundle actin filaments. Thus, our study has identified a fimbrin that may stabilize the actin fringe by cross-linking actin filaments into bundles, which is important for proper tip growth of lily pollen tubes.

INTRODUCTION

Plants rely on a dramatic polar cell growth process, tip growth of the pollen tube within the pistil, to achieve double fertilization. This tip growth process is supported by an elaborate and dynamic actin cytoskeleton (Ren and Xiang, 2007; Cheung and Wu, 2008; Chen et al., 2009; Fu, 2010), which is organized into diverse architectures and performs specific functions in different regions of the pollen tube: the shank, subapex, and apex. In the shank, actin filaments are bundled into long, thick cables, which are arranged in a longitudinal orientation throughout the pollen tube. These provide the main track for transport of organelles and Golgi-driven secretory vesicles and eventually for the cytoplasmic streaming that occurs acropetally along the sides of the tubes and basipetally in the central region (Cai and Cresti, 2009). The organization of actin filaments in the subapex and apex has been controversial for decades because the different methods and markers frequently display inconsistent actin arrangements, such as ring (Kost et al., 1998), funnel (Vidali et al., 2001), subapical mesh (Geitmann et al., 2000; Chen et al., 2002), or basket (Snowman et al., 2002) structures. Recently, a consistent actin arrangement, the dense cortical F-actin called an actin fringe, has been revealed in both live and fixed pollen tubes located in the region 1 to 5 μm from the apex and extending 5 to 10 μm (Lovy-Wheeler et al., 2005; Vidali et al., 2009). Myosin II subfragment 1 decoration and electron microscopy studies have further revealed that short and densely packed parallel actin bundles exist in the subapex of pollen tubes and are more densely packed than those in the shank (Lenartowska and Michalska, 2008). The actin fringe appears to function as the track upon which exocytic vesicles are trafficked from the actin cable to the site of exocytosis, which is independent from cytoplasmic streaming (Bove et al., 2008; Zonia and Munnik, 2008, 2009; Kroeger et al., 2009; Bou Daher and Geitmann, 2011). In the apex, the actin cytoskeleton is less abundant but more dynamic (Fu et al., 2001; Staiger et al., 2010). The tip-localized short actin bundles oscillate and appear at the tip before growth, and the dynamics of short actin bundles are regulated by Rop1At, an Rop GTPase belonging to the Rho family, which indicates that the actin cytoskeleton in the apex is indispensable for ROP-mediated tip growth and polarity controls (Fu et al., 2001; Lee et al., 2008).

The distinct architecture of the actin cytoskeleton in pollen tubes is maintained and regulated by a large set of actin binding proteins (ABPs), many of which are subject to precisely controlled changes in activity and position in time and space. The actin bundles in the shank of pollen tubes are generated from individual microfilaments by the actions of bundling proteins like villins, LIM domain- containing proteins (LIMs), and fimbrins. Villins belong to the villin/gelsolin/fragmin superfamily and comprise at least five isovariants in *Arabidopsis thaliana*. Zhang et al. (2010) proposed that *Arabidopsis* VILLIN5 (VLN5), which is abundant in pollen, harbors filament bundling, barbed-end capping, and Ca^{2+}-dependent severing activities in vitro. In vivo, VLN5 loss of function destabilizes actin and retards pollen tube growth (Zhang et al., 2010). P-135-ABP (Yokota et al., 1998,

[1] Address correspondence to hren@bnu.edu.cn.
The author responsible for distribution of materials integral to the findings presented in this article in accordance with the policy described in the Instructions for Authors (www.plantcell.org) is: Haiyun Ren (hren@bnu.edu.cn).
[C] Some figures in this article are displayed in color online but in black and white in the print edition.
[W] Online version contains Web-only data.
[OA] Open Access articles can be viewed online without a subscription.
www.plantcell.org/cgi/doi/10.1105/tpc.112.099358

2000, 2005; Tominaga et al., 2000) and P-115-ABP (Nakayasu et al., 1998; Yokota et al., 2003) are two villin isoforms isolated from lily (*Lilium longiflorum*) pollen. Immunofluorescence revealed that P-135-ABP is colocalized with microfilament bundles in pollen tubes (Yokota et al., 1998). After injection of P-135-ABP antibody, the transvacuolar strand in living root hair cells disappears, and Alexa-568 phalloidin staining of actin filaments revealed that thick actin bundles in the transvacuolar strand disperse into thin bundles (Tominaga et al., 2000). Another actin-bundling protein, LIM, also plays an important role in pollen tube growth. Wang et al. (2008) isolated a LIM domain–containing protein, LIM1, from lily pollen tubes. Overexpression of Ll-LIM1 significantly retards pollen tube growth and induces abnormal morphology. Biochemical assays verified that Ll-LIM1 is an effective actin bundle factor, and its affinity for F-actin is regulated both by pH and Ca^{2+} (Wang et al., 2008). In addition, it was demonstrated that the three pollen-enriched LIM domain-containing proteins (PLIMs) in *Arabidopsis* are also effective actin bundle factors. Biochemistry assays showed the actin bundling activity of At-PLIMs is inactivated at high pH (pH $\geq$ 6.8, corresponding to the alkaline band in the subapical region of pollen tubes) and, in the case of At-PLIM2c, at high Ca^{2+} levels (Papuga et al., 2010), implying that the PLIMs may participate in the actin bundling in shank of pollen tubes where the optimal pH and Ca^{2+} is maintained. The fimbrin/plastin members are F-actin cross-linking proteins whose binding to actin is mediated by two repeats of highly conserved actin binding domains (Klein et al., 2004). Recently, it has been shown that *Arabidopsis* FIMBRIN5 (At-FIM5) loss of function disrupts the longitudinal arrangement of actin filaments in the shank of pollen tubes, which is associated with the inhibition of pollen tube growth and abnormal morphology (Wu et al., 2010).

On the other hand, in the apical region of the pollen tube, actin filaments reside in certain regions in association with a variety of parameters, including Ca^{2+}, pH, phosphorylation, and phosphoinositides (Franklin-Tong, 1999; Cole and Fowler, 2006; Cheung and Wu, 2008; Zonia, 2010). Therefore, it is assumed that the highly ordered and dynamic actin structure in the subapex and apex is regulated spatially and temporally by several classes of ABPs whose spatiotemporal activities are regulated by specific parameters (Fu, 2010; Staiger et al., 2010). For example, members of the villin/gelsolin family modify actin in a Ca^{2+}-dependent manner. The lily villins P-135-ABP and P-115-ABP mentioned above stabilize actin bundles in the presence of low Ca^{2+} but stimulate depolymerization in regions of elevated Ca^{2+}-calmodulin (Yokota et al., 2005). In addition, P-135-ABP colocalizes with the actin fringe (Lovy-Wheeler et al., 2005). Three different gelsolins, including ABP80 from *Papaver rhoeas* (Huang et al., 2004), ABP41 from *Lilium davidii* (Fan et al., 2004), and ABP29 from lily (Xiang et al., 2007), which are presumably splice variants of villin, actively fragment and depolymerize F-actin and cap the plus ends in regions of elevated Ca^{2+}. Profilin is another Ca^{2+}-responsive ABP that is abundant in pollen of lily and *P. rhoeas* (Vidali and Hepler, 1997; Poulter et al., 2010). It sequesters G-actin and prevents its polymerization into F-actin in regions of elevated Ca^{2+} (Kovar et al., 2000a; Snowman et al., 2002). Lily actin-depolymerizing factor (ADF) is a well-known pH-sensitive ABP. It has been revealed that ADF and actin-interacting protein are located in the cortical actin fringe region. The low $[H^+]$ in the actin fringe may stimulate the fragmenting activity of ADF/actin-interacting protein, and the fragmentation exposes new plus or barbed ends that, in turn, enhance new polymerization of actin, which is necessary to support pollen tube growth (Allwood et al., 2002; Chen et al., 2002; Lovy-Wheeler et al., 2006). Taken together, considering that growing pollen tubes have an intracellular free Ca^{2+} gradient that is highest in the apical dome and an alkaline pH in the actin fringe, it seems that the villin/gelsolin family members profilin and ADF would degrade the existing F-actin in regions of the actin fringe. How then are the short and densely packed parallel actin bundles in the fringe maintained?

In this study, we functionally characterized Ll-FIM1, a fimbrin homolog that is abundant in lily pollen and explored its function in regulating actin dynamics. We proposed that Ll-FIM1 regulates pollen tube tip growth through organization of the actin fringe in the subapical region.

RESULTS

Isolation of *FIM1* cDNA from Lily Pollen

A partial fimbrin-like cDNA was identified by screening a lily pollen cDNA expression library. The full-length cDNA was then obtained by 5′-rapid amplification of cDNA ends approaches. It was found to consist of a 2606-bp segment encoding a putative 690–amino acid protein. The open reading frame was preceded by a 279-bp 5′-untranslated region and followed by a 254-bp 3′-untranslated region. Comparison of the protein sequences showed that the peptides shared high amino acid identity with fimbrin/plastin family proteins, such as human T-plastin, yeast SAC6P, and At-FIM5 (see Supplemental Figure 1 online). Hereafter, the protein is named Ll-FIM1.

To analyze the relationship between Ll-FIM1 and fimbrin homologs in *Arabidopsis*, rice (*Oryza sativa*), maize (*Zea mays*), and moss (*Physcomitrella patens*), a phylogenetic tree was generated using the core domain (CH1-CH4) sequences of Ll-FIM1 and fimbrins from various species (see Supplemental Figure 2 and Supplemental Data Set 1 online). Based on unweighted pair group method- determined analysis, it was revealed that Ll-FIM1 has a close relationship with *Arabidopsis* FIM5 and FIM3.

RT-PCR analysis was conducted to detect the expression patterns of Ll-*FIM1*. The relative expression level of Ll-*FIM1* in each sample was determined with gene-specific primers. As shown in Figure 1, Ll-*FIM1* transcripts were present in all tissues and organs tested and abundant in dried pollen grains and pollen tubes, as well as leaves and sepals. Amplification of *ACTIN* served as a loading control.

FIM1 Is Localized at Actin Filaments in Lily Pollen Tubes

To examine the subcellular localization of Ll-FIM1 protein in pollen tubes, a polyclonal antibody against the C-terminal region of Ll-FIM1 corresponding to amino acids 620 to 690 was raised in rabbit, and the cross-reactivity of the antibody with recombinant Ll-FIM1 protein and At-FIM5 protein was examined. This antibody

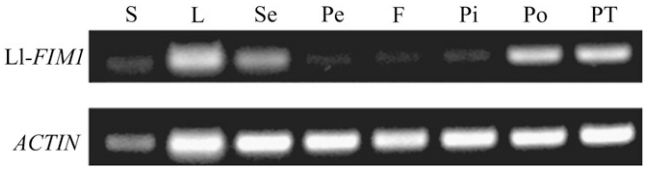

Figure 1. Expression of FIM1 in Different Tissues of Lily.

Stems (S), leaves (L), sepals (Se), petals (Pe), filaments (F), pistils (Pi), pollen (Po), and pollen tubes (PT) were collected from lily after flowering and used for total RNA isolation. RT-PCR analysis of Ll-*FIM1* expression was performed with primers specific to Ll-*FIM1*, with primers specific to *ACTIN* as a loading control.

reacted strongly with recombinant Ll-FIM1 protein but not with At-FIM5 protein (Figure 2A). Furthermore, immunoblotting demonstrated that the antibody was specific for a band estimated to be ~80-kD, which is identical to the molecular mass of Ll-FIM1 in the crude protein extracts of lily pollen (Figure 2B), confirming the specificity of the polyclonal antibody. Then, the antibody was used to examine the subcellular localization of FIM1 in pollen tubes of lily.

In the immunofluorescence experiments, pollen tubes were chemically fixed and actin filaments were labeled by Alexa-568 phalloidin. Under the confocal microscope, we observed that the Ll-FIM1 protein was located at the actin fringe structure in subapex (Figure 2C, a1 to a3) and along with the actin bundles in the shank (Figure 2C, b1 to b3). Following treatment of the pollen tubes with 1 μM latrunculin B (LatB) and resulting disassembly of the actin filaments, the Ll-FIM1–labeled bundle structures become fragmented as well (Figure 2C, c1 to c3). Moreover, Ll-FIM1 was also dispersed throughout the cytoplasm (Figure 2C, b3 and c3). The colocalization between Ll-FIM1 and actin filaments in the tip and shank areas of chemically fixed pollen tubes was analyzed and quantified using the Pearson-Spearman correlation (PSC) plug-in for ImageJ (French et al., 2008). The linear Pearson (r_p) and the nonlinear Spearman's rank (r_s) correlation coefficient for the pixels representing the fluorescence signals in both channels were calculated. The values indicate the level of colocalization ranging from +1 for perfect colocalization to −1 for negative correlation (French et al., 2008). Our results showed that, in the tip and shank regions, both Pearson and Spearman *r* values were high (mean ± SE, the tip: $r_p = 0.574 \pm 0.058$, $r_s = 0.572 \pm 0.059$; the shank: $r_p = 0.528 \pm 0.05$, $r_s = 0.5 \pm 0.056$. $n \geq 10$), indicating strong colocalization of Ll-FIM1 and actin filaments. To verify further the relative extent of the colocalization between FIM1 and the actin filaments in chemically fixed lily pollen tubes, we also applied a colocalization algorithm that was used specifically for actin filaments and ABPs (Poulter et al., 2010). The data showed that Ll-FIM1 was colocalized with the actin filaments (mean ± SE, the tip: 65.37% ± 9.44%; the shank: 70.67% ± 5.37%; $n \geq 10$). In addition, we also applied the rapid freeze fixation method that has been shown to preserve the actin fringe structure well (Lovy-Wheeler et al., 2005). Antibodies directed against actin and Ll-FIM1 were used, and the dual-immunolabeling result showed strong colocalization in the subapex of pollen tubes (see Supplemental Figure 3 online). These findings reveal that Ll-FIM1 is concentrated at actin filament bundles in pollen tubes.

Microinjection of Ll-FIM1 Antibody in Pollen Tubes Retards the Growth Rate and Destroys the Actin Fringe Structure in the Subapex

To explore the biological function of Ll-FIM1 in pollen tube elongation, we performed microinjection experiments with the specific Ll-FIM1 antibody, a technique that has been shown previously to be effective in exploring the function of proteins during pollen tube growth (Lin and Yang, 1997). We microinjected Ll-FIM1 antibody into growing pollen tubes cultured on low-melting agarose pollen germination medium and observed the subsequent tube growth. As shown in Figures 3A and 3B, microinjection of Ll-FIM1 antibody significantly reduced the growth rate in a dose-dependent manner (6.37 ± 1.34 μm/min, 0.3 mg/mL antibody; 5.08 ± 1.28 μm/min, 0.5 mg/mL antibody; and 1.64 ± 0.59 μm/min, 1 mg/mL antibody) within 10 min after the completion of the microinjection compared with the control (10.96 ± 1.33 μm/min) (Figures 3A and 3B). These negative effects were specific for the antibody, given that when identical microinjection experiments were performed using buffer or BSA, the injected pollen tubes retained normal growth rates (Figures 3A and 3B). In addition, we selected cytosolic organelles in the shank of pollen tubes that exhibited continuous movements to measure the velocity of cytoplasmic streaming. This analysis showed that the velocity of cytoplasmic streaming was significantly reduced in antibody-injected pollen tubes (see Supplemental Figure 4 online).

To investigate whether the growth phenotype for the antibody injection correlated with an altered actin cytoskeleton, we observed the actin filaments of antibody-injected pollen tubes after chemical fixation with Alexa-488 phalloidin as a probe. As can be seen in Figure 3C, the control pollen tubes showed a multitude of parallel actin bundles in the shank and the actin fringe in the subapical region (Figure 3C, a and a'; see Supplemental Figure 5A, a, online). Although the thick actin bundles in the shank were still visible after microinjection of Ll-FIM1 antibody, the actin fringe close to the tip had been impaired (Figure 3C, b and b'; see Supplemental Figure 5A, b to d, online). To quantify these changes, two statistical parameters, skewness and density, for measuring the extent of bundling and abundance of actin filaments were applied (Higaki et al., 2010; Henty et al., 2011). As shown in Supplemental Figures 5B and 5C online, in the tip area of antibody-injected pollen tubes, the average skewness and occupancy values were significantly decreased in comparison to the buffer-injected pollen tubes. However, there was no significant difference in density or bundle level in the shank (see Supplemental Figures 5D and 5E online). These results reveal that the Ll-FIM1 protein mainly participates in the formation of the actin fringe in the subapical region of pollen tubes.

The Morphology of Pollen Tubes in *Arabidopsis fim5* Mutants Is Abnormal during the Early Stage but Recovers Later

At-FIM5 is a fimbrin homolog protein that is abundant in *Arabidopsis* pollen, and among the *Arabidopsis* fimbrins, it is the

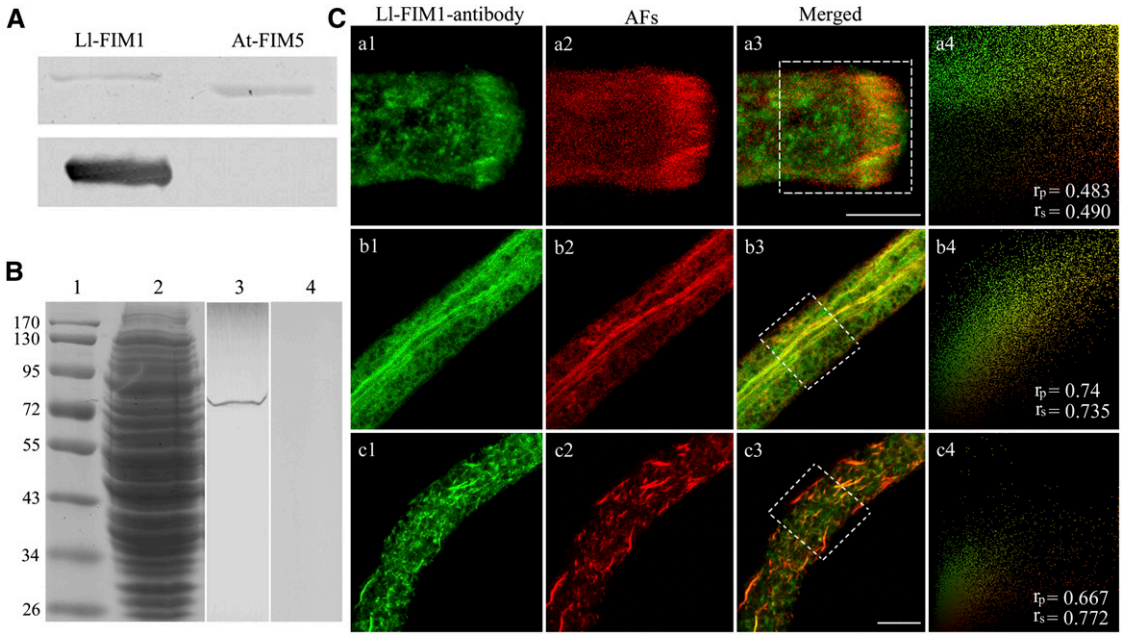

Figure 2. FIM1 Colocalizes with Actin Filaments in Lily Pollen Tubes.

(A) Immunoblot analysis showed that the antibody specifically recognized recombinant Ll-FIM1 but did not recognize recombinant At-FIM5. The top image shows a Coomassie blue–stained gel of recombinant Ll-FIM1 and At-FIM5, respectively; the bottom image shows the corresponding protein gel blot probed with the affinity-purified anti-Ll-FIM1 antibody.

(B) Immunoblot analysis showed that the antibody specifically recognized FIM1 from the protein extracts of lily pollen tubes. Marker, lane 1; Coomassie blue–stained gel of the protein extracts of pollen tubes, lane 2; the corresponding protein gel blot probed with affinity-purified anti-Ll-FIM1 antibody, lane 3; and preimmune serum, lane 4.

(C) Dual-fluorescence localization with Ll-FIM1 antibody (a1, b1, and c1) and phalloidin (a2, b2, and c2) in lily pollen tubes. Actin was observed as the red fluorescence of phalloidin and Ll-FIM1 as the green fluorescence of fluorescein isothiocyanate. The images are projections. (a1) Ll-FIM1 protein was focused in the subapex of the pollen tube; (b1) Ll-FIM1 protein was visible on large bundles along the shank of the pollen tube; (c1) the distribution of Ll-FIM1 protein after treatment with LatB; (a2) and (b2) The distribution of actin filaments (AFs) in lily pollen tube; (c2) AFs became fragmented after treatment with LatB; (a3), (b3), and (c3) overlay images showed that the Ll-FIM1 protein colocalized with AFs in lily pollen tubes. Intensities of fluorescent signals from the hatched boxes in (a3), (b3), and (c3) are depicted in a scatterplot at the right side of each row (a4, b4, and c4), and the calculated PSC values are given in the bottom right corner. The two signals showed strong colocalization. Bars = 10 μm.

most closely related to Ll-FIM1. In the core CH domains (CH1 to CH4), 81.4% (407/500) and 98% (490/500) of amino acids are identical or similar in Ll-FIM1 and At-FIM5. To investigate further the function of fimbrin isoforms that are preferentially expressed in pollen tubes, we explored the phenotype of the *Arabidopsis fim5-1* mutant (Wu et al., 2010) in detail. In addition to the pollen germination defects reported by Wu et al. (2010), we further found that in the early stage of pollen tube growth, mutant tubes frequently exhibited partial depolarization, and the tubes were larger in diameter than those of wild-type Columbia-0 (Col-0) plants (Figure 4A). Impressively, a majority of the mutant pollen tubes (>85%) recovered their normal morphology after being cultured for more than 9 h (Figure 4A). These observations were supported by statistical analysis (Figure 4B).

To verify further the above phenotype, we examined the morphology of wild-type and *fim5* pollen tubes in vivo. Wild-type pistils were pollinated with either wild-type pollen or *fim5* pollen, then fixed and stained with aniline blue. We then observed that compared with the wild type, the *fim5* pollen tubes grew with a larger diameter in the early stage. However, as germination time increased, the enlarged base of mutant pollen tubes recovered and gradually became thinner, which was consistent with the phenotype we observed in vitro (Figure 4D).

We further analyzed the growth dynamics of wild-type and *fim5* pollen tubes by time-lapse video microscopy. The growth rate of growing pollen tubes was measured every 30 min. Throughout the growth period, *fim5* pollen tubes grew more slowly than did those of the wild type (Figure 4C; see Supplemental Figure 6 online), which resembled the phenotype of lily pollen tubes that were microinjected with Ll-FIM1 antibody. Moreover, statistical analysis showed that the growth rate of *fim5* pollen tubes was significantly slower than those of the wild type, even though the morphology had recovered (see Supplemental Figure 6 online).

Loss of Function of At-FIM5 Profoundly Affects the Cortical Actin Fringe

To visualize the correlation of arrangements of actin cytoskeleton with the abnormal pollen tube tip growth in *fim5* mutants, we

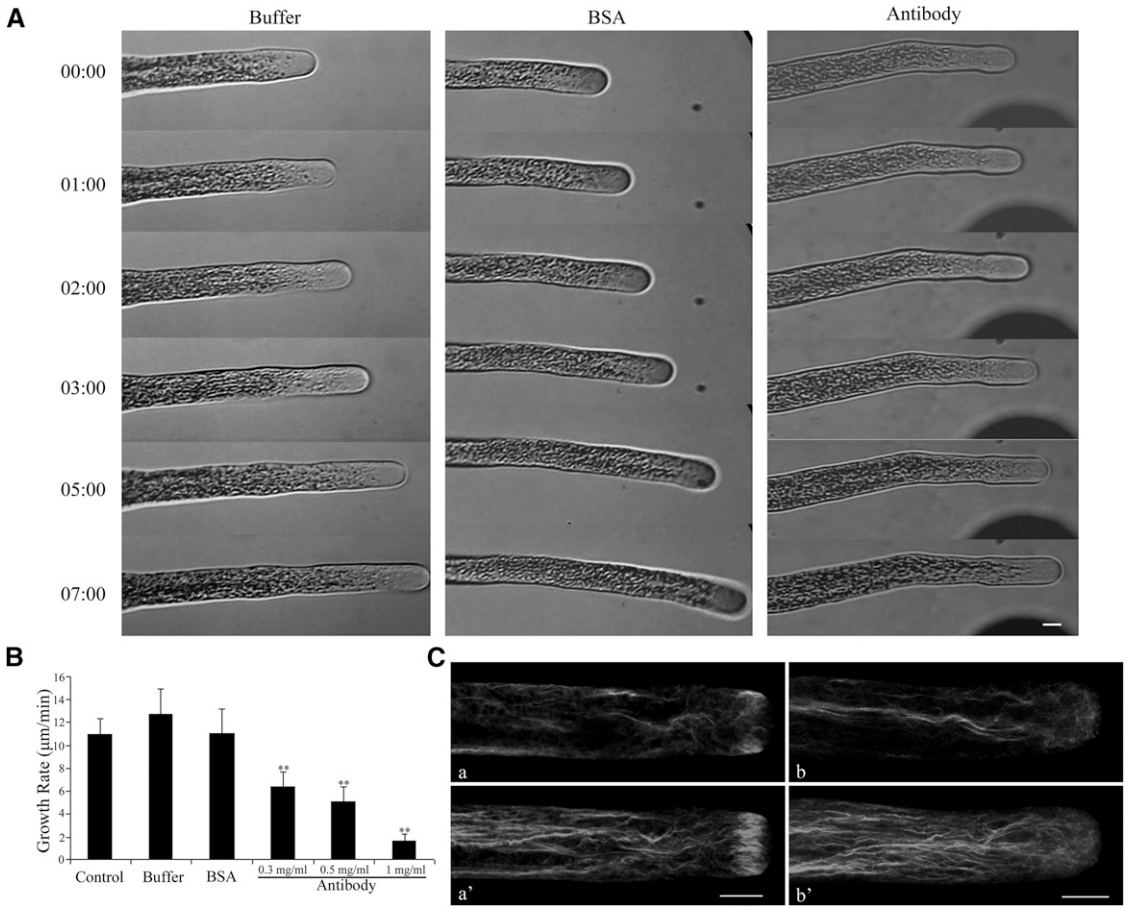

Figure 3. Time-Lapse Micrographs Illustrate Effects of Antibody Injection on Lily Pollen Tube Growth.

(A) Growing lily pollen tubes were microinjected with LI-FIM1 antibody, BSA, or control buffer, as indicated. After 5 min of recovery, micropipette tips were slowly removed from the pollen tube, and the pollen tube was observed 10 min following injection. Time notated in minutes and seconds (mm:ss). Bar = 10 μm.

(B) The growth rate decreased significantly in the pollen tubes that were injected with antibody. Error bars represent mean ± SE (**P < 0.01, by Student's *t* test, $n \geq 15$ per group).

(C) F-actin organization in antibody-injected pollen tubes and control pollen tubes. About 10 min after injection, cells were chemically fixed and stained with 200 nM Alexa-488 phalloidin. (a) and (a') Control cell; (b) and (b') cell injected with LI-FIM1 antibody. All cells were visualized by confocal microscopy. (a) and (b) show medial confocal optical sections. The images in (a') and (b') are projections. Bar = 10 μm.

labeled pollen tubes from wild-type *Arabidopsis* and the *fim5* mutant with Alexa-488 phalloidin. It was remarkable that in the subapex of wild-type pollen, the actin fringe was prominent in both the early and late stages (Figures 5A, a, and 5B, a). By contrast, in the early stage *fim5* pollen tubes, the actin fringe was impaired and, simultaneously, the disarranged actin bundles protruded into the tips (Figure 5A, b). However, even after the diameter recovery in the late stage, the actin fringe structures remained impaired despite the fact that the parallel actin bundles had returned to normal in the shank (Figure 5B, b and c). Collectively, over 98% (54/55) of the pollen tubes in the wild type had obvious actin fringe structures, but in *fim5* mutants, up to 90% (36/40) had no discernible actin fringe structures. To quantify actin filaments in the tip and the shank region, skewness and density parameters were used in pollen tubes of the wild type and *fim5* mutant at both early and late stages. In comparison to the wild type, the actin arrays in both tip and shank areas of *fim5* mutants were less bundled during the early stage (Figure 5C). The average occupancy value of *fim5* mutants was not lower in the tip region, but it was even higher in the shank region (Figure 5E). This further supports that there are fewer actin bundles in *fim5* pollen tubes if the overall amount of actin remains the same in the mutant. The skewness and occupancy value measurements were also found to be inversely correlated by Henty et al. (2011). In the late stage, after the morphology recovered, there was a remarkable decrease in average skewness and occupancy values in tip region of *fim5* mutants in comparison to the wild type. However, for both skewness and occupancy values in the shank, there was no significant difference between wild type and *fim5* pollen (Figures 5D and 5F). These results indicate that At-FIM5 contributes to the organization of both actin fringe and the long actin bundles

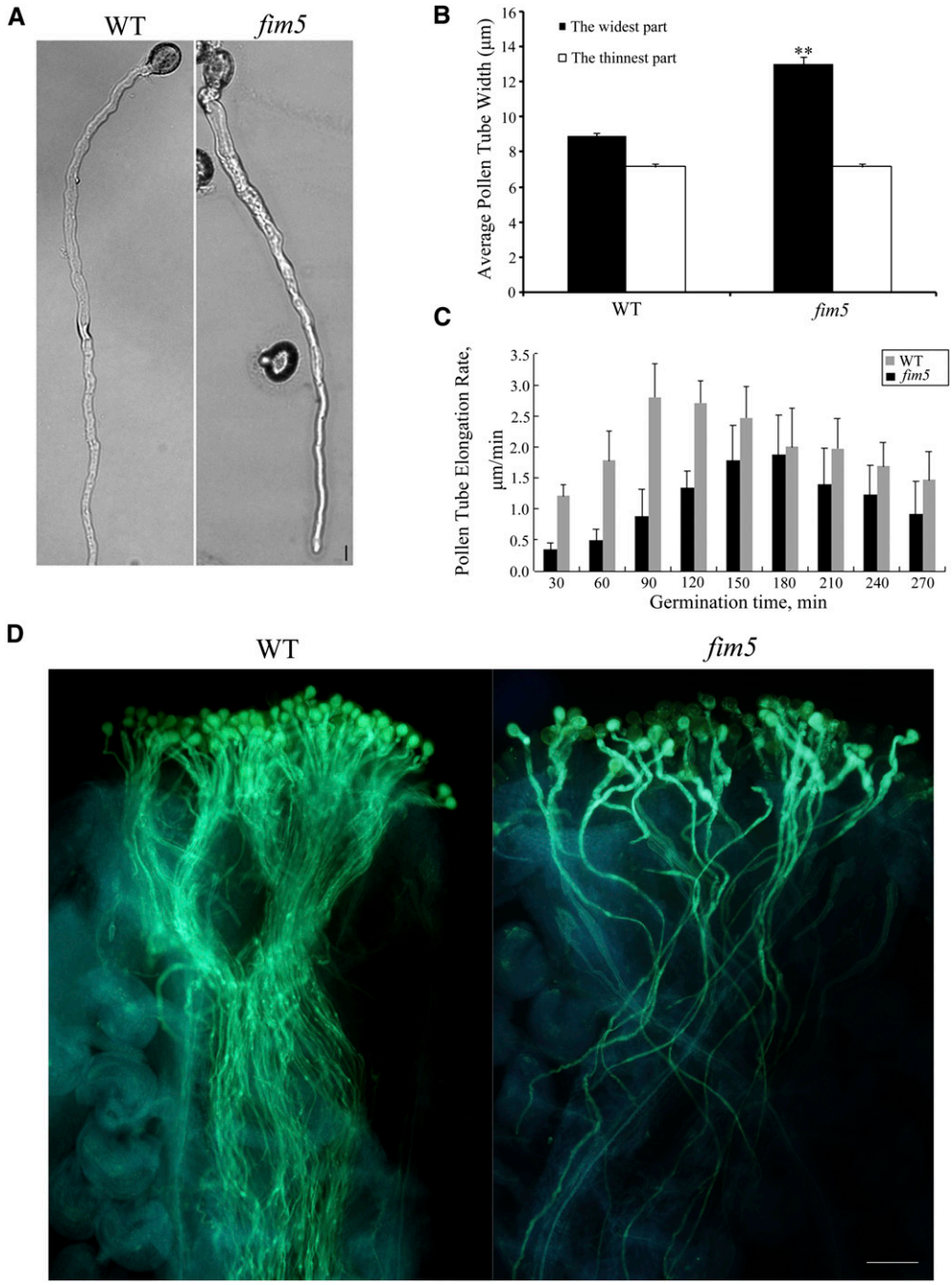

Figure 4. The Diameter of *Arabidopsis fim5* Pollen Tubes Is Irregular in Early Stages but Recovers Later.

(A) Representative image of pollen tubes from wild-type (WT) Col-0 and *fim5* mutants germinating on *Arabidopsis* pollen germination medium for 12 h. Bar = 10 μm.

(B) The widest and thinnest parts of the pollen tubes from wild-type Col-0 and *fim5* mutants were measured. The diameter of the widest parts from *fim5* mutants was significantly larger compared with wild-type Col-0 (**P < 0.01, by *t* test, $n \geq 40$ per group), whereas there was no difference in the thinnest parts. Error bars represent mean ± SE.

(C) The growth rate of *fim5* pollen tubes decreased compared with the wild type. Germination time refers to the growth time of pollen tubes. Error bars represent mean ± SE ($n \geq 10$ per group).

(D) Pollen grains from wild-type Col-0 and *fim5* mutants were used to pollinate wild-type stigmas. Pollen tubes were visualized by aniline blue staining. Bar = 1 mm.

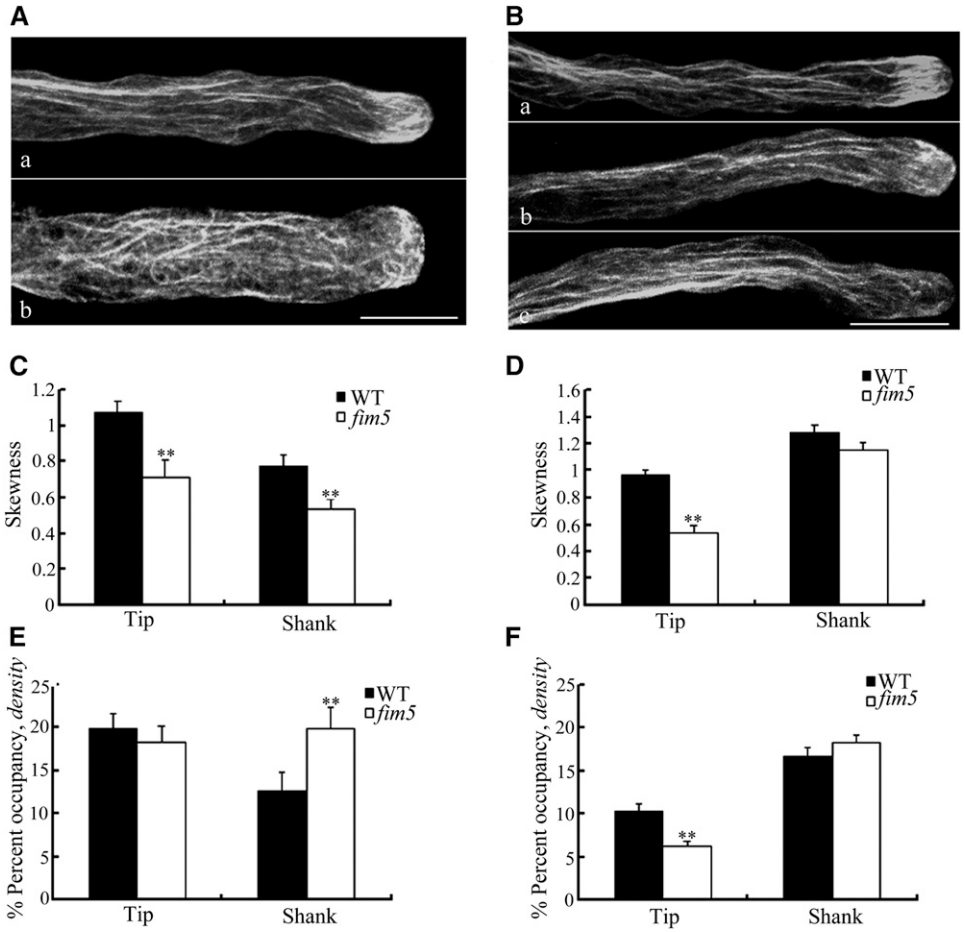

Figure 5. F-Actin Distribution in Pollen Tubes of Wild-Type *Arabidopsis* and *fim5* Mutants.

(A) Actin organization was disturbed in *fim5* mutants in the early stage (growing time ≤6 h), and actin cables protruded into the extreme tips. (a) The wild type; (b) *fim5*. Bar = 10 μm.

(B) The actin fringe structure was prominent in pollen tubes of the wild type (a), whereas this structure was not discernable in *fim5* mutants (b and c) at the late stage (the culturing time was 12 h). Bar = 10 μm.

(C) and **(D)** Quantitative analysis of the extent of actin bundling in the tip and shank areas at the early stage **(C)** and the late stage **(D)** based on skewness. Pollen tubes of *fim5* mutants had significantly decreased average skewness values in both tip and shank areas (**P < 0.01, by *t* test, $n \geq 20$ per group) **(C)**. Pollen tubes of *fim5* mutants had significantly decreased average skewness values in the tip area (**P < 0.01, by *t* test, $n \geq 40$ per group), and there was no significant difference in the shank area (P > 0.05, by *t* test, $n \geq 28$ per group) **(D)**. Error bars represent mean ± SE. WT, the wild type.

(E) and **(F)** Quantitative analysis of actin density in the tip and shank areas at the early stage **(E)** and the late stage **(F)**. Pollen tubes of *fim5* mutants had significantly increased average occupancy values in the shank area (*P < 0.01, by *t* test, $n \geq 20$ per group), and there was no significant difference in tip area (P > 0.05, by *t* test, $n \geq 20$ per group) **(E)**. Pollen tubes of *fim5* mutants had significantly decreased average occupancy values in the tip area (**P < 0.01, by *t* test, $n \geq 40$ per group), and there was no significant difference in the shank area (P > 0.05, by *t* test, $n \geq 28$ per group) **(F)**. Error bars represent mean ± SE.

in the early stage, but in the late stage, it mainly participates in the formation of the actin fringe.

Expression of GFP-LI-FIM1 Rescues the *fim5* Phenotype

As mentioned above, among the *Arabidopsis* fimbrins, LI-FIM1 shares the most identity with At-FIM5, which is also abundant in pollen. We examined the ability of LI-FIM1 to rescue the *Arabidopsis fim5* mutant phenotype. The *fim5pro:GFP:LI-FIM1* (for a green fluorescent protein fusion) vector was constructed, and complementation experiments were performed by driving expression of GFP-LI-FIM1 in *fim5* mutant plants. In homozygous *fim5* mutant plants heterozygous for expression of GFP-LI-FIM1, half of the pollen grains expressed GFP-LI-FIM1 and half did not express GFP-LI-FIM1. This allowed us to compare the mutant pollen tubes with the mutant pollen tubes expressing the GFP-LI-FIM1 rescue construct. As shown previously, the *fim5* pollen (without expression of GFP-LI-FIM1) formed short, abnormal pollen tubes, as the arrow indicates (Figure 6A). By contrast, the *fim5* pollen expressing GFP-LI-FIM1 formed long pollen tubes of a uniform diameter, and these pollen tubes were similar in appearance to the wild-type pollen tubes (Figure 6A).

The average lengths and widths of pollen tubes from *fim5* mutant plants homozygous for expression of GFP-LI-FIM1 were similar to those of the wild-type Col-0 plants (Figures 6B and 6C), indicating that defects in male gametophytes were indeed rescued by GFP-LI-FIM1 expression. In addition, the pollen tube elongation rate of complemented lines also returned to normal (see Supplemental Figure 6 online). Moreover, to test whether GFP-LI-FIM1 could reconstruct the actin fringe, we compared the actin fringe in pollen tubes of wild-type *Arabidopsis*, *fim5* mutants, GFP-At-FIM5–complemented lines and GFP-LI-FIM1–complemented lines, respectively. As shown in Figure 7A, pollen tubes of the GFP-At-FIM5–complemented lines and GFP-LI-FIM1–complemented lines showed prominent actin fringe. Quantitative analysis showed the average occupancy value in tip of GFP-LI-FIM1–complemented pollen was similar to that of GFP-At-FIM5–complemented pollen, and both of them could rescue the actin fringe of *fim5* mutants (Figure 7B). In addition, for occupancy values in the shank, there was no significant difference between wild-type and complemented lines (mean ± SE: 13.6% ± 2.1%, wild type; 15.3% ± 3.1%, GFP-At-FIM5–complemented lines; and 12.7% ± 1.5%, GFP-LI-FIM1–complemented lines, $n \geq 30$, $P > 0.05$). Therefore, we concluded that LI-FIM1 could functionally replace the endogenous At-FIM5 protein.

Results from complementation experiments indicated that the GFP-LI-FIM1 protein was functional, providing suitable means to characterize the subcellular localization of LI-FIM1 in *Arabidopsis* pollen tubes. As shown in Figure 7A (d to f), GFP-LI-FIM1 was obviously colocalized with the actin fringe stained with Alexa-568 phalloidin in the subapex of the GFP-LI-FIM–complemented pollen tube. Besides, it was also colocalized with the actin bundles in the shank and distributed throughout the cytoplasm. In order to quantify the colocalization between GFP-LI-FIM1 and the actin fringe, we calculated the r_p and the r_s PSC for the pixels that represent the fluorescence signals in both channels, with pollen tubes expressing GFP as a negative control. Supplemental Figure 7 online displays the representative fluorescence images. The r_p and r_s correlation coefficients were low in the negative control (mean ± SE, r_p = 0.059 ± 0.05; r_s = 0.108 ± 0.054, n = 10). By contrast, GFP-LI-FIM1 revealed a high degree of fluorescence signal overlap with the actin fringe in complemented lines (mean ± SE, r_p = 0.424 ± 0.029; r_s = 0.381 ± 0.039, n = 10) and a modest degree in GFP-LI-FIM1 overexpression lines (mean ± SE, r_p = 0.287 ± 0.054; r_s = 0.303 ± 0.053, n = 10). To verify further the relative extent of the colocalization between GFP-LI-FIM1 and the actin fringe, we also applied the colocalization algorithm used by Poulter et al. (2010). The data showed that the association of GFP with the actin fringe was relatively low (15% ± 4.01%), whereas GFP-LI-FIM1 showed higher levels of colocalization in complemented lines (66.45% ± 7.07%), further demonstrating the colocalization of GFP-LI-FIM1 with the actin fringe. In GFP-LI-FIM1 overexpression pollen tubes, the extent of colocalization (28% ± 2.74%) was higher than in the negative control, but

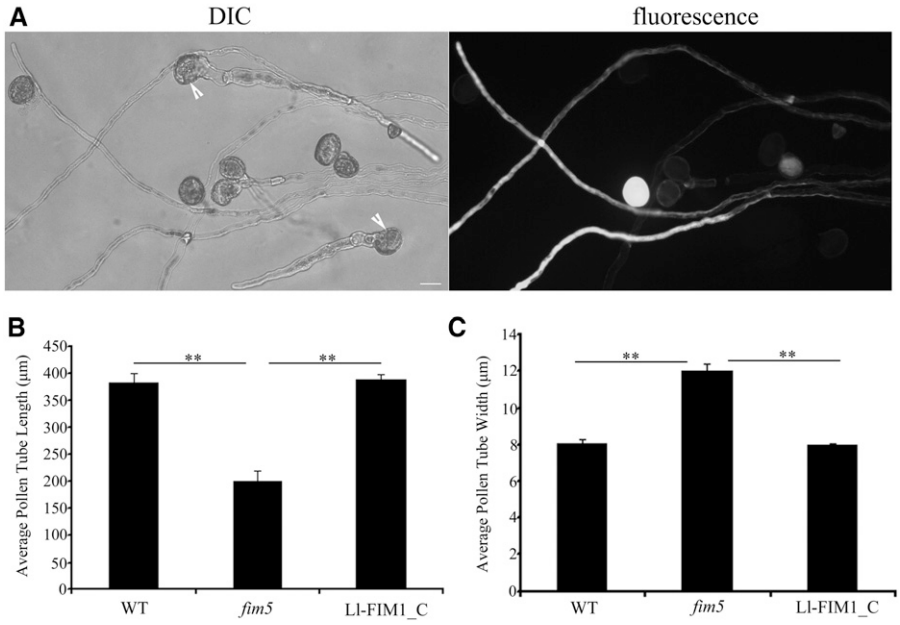

Figure 6. GFP-LI-FIM1 Complements the Phenotype of *Arabidopsis fim5* Mutants.

(A) Pollen from homozygous mutant plants heterozygous for expression of GFP-LI-FIM1. Arrows indicate *fim5* mutant pollen not expressing GFP-LI-FIM1. DIC, differential interference contrast. Bar = 10 μm.

(B) Quantitative analysis of pollen tube lengths of the wild type (WT), *fim5* mutants, and GFP-LI-FIM1–complemented lines (LI-FIM1_C) after 7 h culture. Error bars represent mean ± SE (**$P < 0.01$, by *t* test, $n \geq 35$ per group).

(C) Quantitative analysis of the diameter at the widest parts of the wild type, *fim5* mutants, and GFP-LI-FIM1–complemented lines (LI-FIM1_C) after 7 h culture. Error bars represent mean ± SE (**$P < 0.01$, by *t* test, $n \geq 35$ per group).

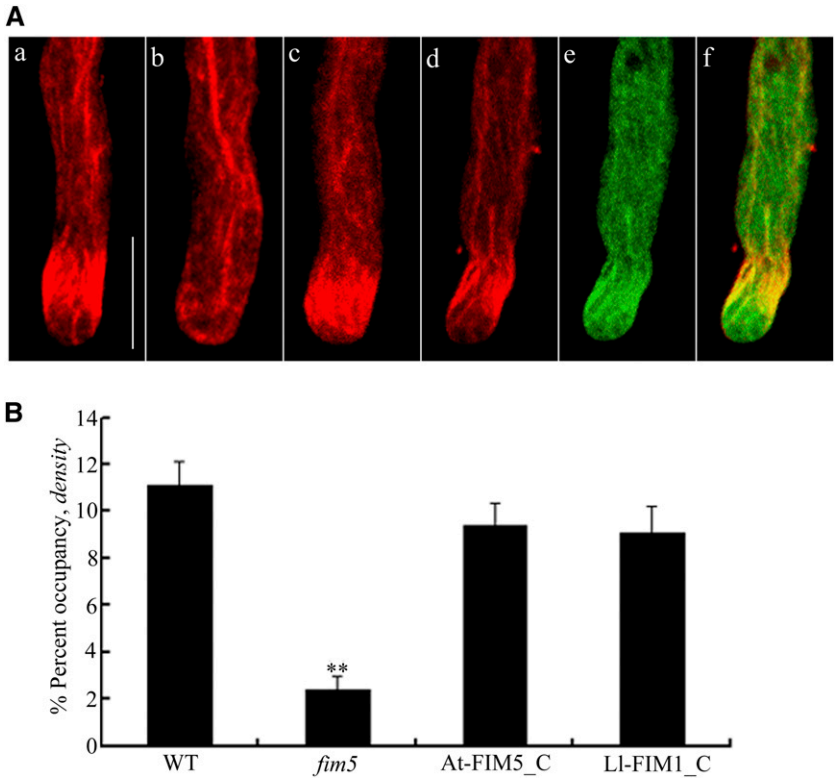

Figure 7. GFP-Ll-FIM1 Rescues the Actin Fringe in Complemented Lines.

(A) The actin organization in complemented pollen tubes showed a prominent subapical actin fringe. The distribution of actin filaments in the wild type (a), the *fim5* mutant (b), the GFP-At-FIM5–complemented line (c), and the GFP-Ll-FIM1–complemented line (d). Actin was observed as the red fluorescence of phalloidin. (e) The distribution of GFP-Ll-FIM1 protein in complemented pollen tubes. (f) Overlay image showed that the Ll-FIM1 protein localized at the actin fringe in complemented pollen tubes. Bar = 10 μm.

(B) Quantitative analysis of the microfilament density in tip region of pollen tubes from the wild type (WT), *fim5* mutants, GFP-At-FIM5–complemented lines (At-FIM5_C), and GFP-Ll-FIM1–complemented lines (Ll-FIM1_C). Error bars represent mean ± SE (**P < 0.01, by *t* test, $n \geq 40$ per group). The microfilament density of pollen tubes of GFP-Ll-FIM1–complemented lines was similar to that of the GFP-At-FIM5–complemented lines.

much lower than that of the complemented lines. The dispersed subcellular localization in overexpression lines might be due to lack of docking site that is occupied by endogenous fimbrins.

In addition, we also examined the cellular distribution of Ll-FIM1 in live growing pollen tubes of GFP-Ll-FIM1–complemented lines. Pollen tubes expressing GFP were used as a negative control. It was shown by time-lapse imaging that fimbrin dynamically decorated a structure resembling the actin fringe in the subapical region of most GFP-Ll-FIM1–complemented pollen tubes (90%, 18/20). A representative picture is shown in Supplemental Figure 8 online. This result establishes that the GFP-Ll-FIM1 protein colocalizes with the actin fringe.

The Recombinant Ll-FIM1 Binds Directly to Actin Filaments

Our experiments presented above show that Ll-FIM1 localizes at the actin filaments and mainly regulates the actin fringe structure in pollen tubes. Therefore, in vitro biochemical experiments were performed to determine the direct actin binding activity of Ll-FIM1. Full-length Ll-FIM1 with a 6-His tag in its C terminus was expressed in *Escherichia coli* and purified by affinity chromatogram. A high-speed cosedimentation assay (Figure 8A) showed that the recombinant Ll-FIM1 cosedimented with actin filaments. Statistical analysis showed that the ratio of the amount in the pellet to the amount in the supernatant was increased from 19.4% ± 0.9% to 36.4% ± 1.7% (n = 3) when actin was added, which indicated that Ll-FIM1 could bind directly to actin filaments. To determine the apparent equilibrium dissociation constant (K_d) values of Ll-FIM1, increasing concentrations of phalloidin-stabilized F-actin were incubated with 0.8 μM Ll-FIM1. Following centrifugation at high speed, the percentage of Ll-FIM1 in the pellet was determined by densitometric analysis, and the concentration of bound Ll-FIM1 was plotted against the concentration of actin and fitted with a hyperbolic function. The average dissociation constant (K_d) value for Ll-FIM1 binding to F-actin was 0.69 ± 0.2 μM (mean ± SD, n = 4), and a representative experiment is shown in Figure 8B, indicating that Ll-FIM1 binds to actin filaments with high affinity.

Ll-FIM1 Bundles Actin Filaments in a Ca^{2+}-Independent and pH-Dependent Manner

Because F-actin bundling activity is a common feature of fimbrin family proteins, we also tested whether Ll-FIM1 was capable of

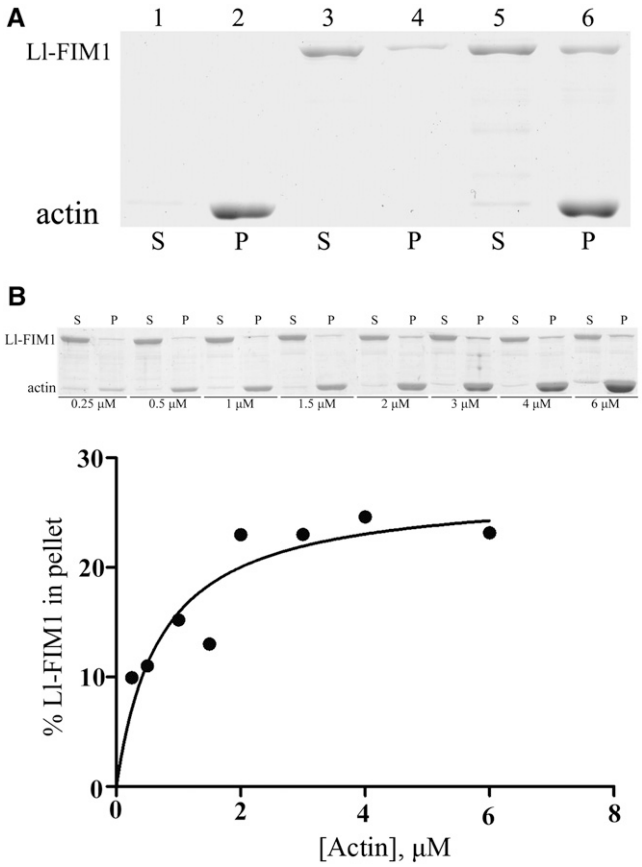

Figure 8. Ll-FIM1 Can Bind Actin Filaments Directly.

(A) A high-speed cosedimentation assay was used to determine Ll-FIM1 binding to F-actin. A mixture of 3 μM F-actin and 1 μM Ll-FIM1 was centrifuged at 200,000*g*. The resulting supernatants (S) and pellets (P) were subjected to SDS-PAGE and Coomassie stained. Samples are as follows: lane 1, actin alone supernatant; lane 2, actin alone pellet; lane 3, Ll-FIM1 alone supernatant; lane 4, Ll-FIM1 alone pellet; lane 5, actin plus Ll-FIM1 supernatant; lane 6, actin plus Ll-FIM1 pellet.

(B) Increasing concentrations of phalloidin-stabilized F-actin were mixed with 0.8 μM Ll-FIM1. The concentration of bound Ll-FIM1 was plotted against the concentration of actin and fitted with a hyperbolic curve. For this representative experiment, the calculated dissociation constant (K_d) was 0.73 μM.

bundling actin filaments using a low-speed cosedimentation assay and fluorescence microscopy. As shown in Figure 9A, preassembled actin (3 μM) was incubated with increasing concentrations of Ll-FIM1 (0.25 to 5 μM) and centrifuged for 30 min at 13,500*g*. Samples were analyzed by SDS-PAGE, and the pelleted actin was quantified by densitometric analysis (Figure 9A). In the absence of Ll-FIM1, very little actin was detected in the pellet. However, in the presence of Ll-FIM1, the amount of actin in the pellet increased proportionally to the Ll-FIM1 concentration, indicating that Ll-FIM1 induced the formation of a higher-order F-actin structure. Also, the actin bundling activity of Ll-FIM1 was confirmed by fluorescence observation of actin filaments visualized through Alexa-488 phalloidin staining. Actin filaments appeared as single filaments in the absence of Ll-FIM1 (Figure 9B, a) but organized into filament bundles with the addition of 1 μM Ll-FIM1 (Figure 9B, b).

It has been reported that the pH in the actin fringe area is alkaline, but in the shank is acidic (Feijó et al., 1999), and there is a tip-focused Ca^{2+} gradient present in growing pollen tubes (Rathore et al., 1991; Pierson et al., 1994). We then tested how Ll-FIM1 responded to different concentrations of calcium and pH values. To determine whether the actin bundling activity of Ll-FIM1 was regulated by Ca^{2+}, 3 μM prepolymerized actin filaments were incubated with 1 μM Ll-FIM1 in the presence of various concentrations of Ca^{2+} for 1 h. As shown in Supplemental Figure 9 online, the actin pellet did not show a significant difference under varying concentrations of Ca^{2+}, suggesting that Ll-FIM1 bundles actin filaments in a Ca^{2+}-independent manner. This observation is consistent with other plant fimbrins reported in the literature (Kovar et al., 2000b; Wu et al., 2010). In pH regulation tests, increasing concentrations of Ll-FIM1 were incubated with actin under buffering systems of pH 6.2 and 7.4, respectively, according to Papuga et al. (2010). The amount of pelleted actin increased proportionally to the Ll-FIM1 concentration in both pH 6.2 buffer and pH 7.4 buffer (see Supplemental Figure 10A online). Quantitative analysis suggested the amount of pelleted actin in buffering systems of pH 6.2 was significantly higher than the amount in pH 7.4, suggesting that Ll-FIM1 bundles actin filaments in a pH-sensitive manner (see Supplemental Figure 10B online).

DISCUSSION

With the development of techniques in recent years, it has been revealed that growing pollen tubes, especially those of the lily, consistently show a prominent actin fringe that resides in the cortical cytoplasm and is closely associated with the plasma membrane in the subapex (Lovy-Wheeler et al., 2005). In the actin fringe, some actin filaments are organized in closely packed and longitudinally oriented bundles, and some form curved bundles that are adjacent to the cell membrane (Lenartowska and Michalska, 2008). However, the ABPs that participate in the maintenance of the actin bundles in the actin fringe are still poorly understood.

Several ABPs, such as formins, villins, LIMs, and fimbrins, are commonly assumed to be involved in the formation and/or the maintenance of actin bundles in plants (Thomas et al., 2009). Among these ABPs, the formins expressed in pollen tubes act more as actin nucleators rather than as actin bundlers. For example, *Arabidopsis* FORMIN HOMOLOGY3 is an actin nucleation factor responsible for the formation of longitudinal actin cables in pollen tubes (Ye et al., 2009); *Arabidopsis* FORMIN HOMOLOGY5 performs actin nucleating activity in the subapical area (Cheung et al., 2010). Villins and LIMs, which are tightly regulated by pH and/or Ca^{2+}, are the prime candidates for regulating actin fringe remodeling during pollen tube elongation. It has been demonstrated that most plant villins exhibit severing activities at high calcium levels and bundling activities at low calcium levels in vitro (Yokota et al., 2003, 2005; Khurana et al., 2010; Zhang et al., 2010). Therefore, it is possible that during the oscillating growth of pollen tubes, villin homolog

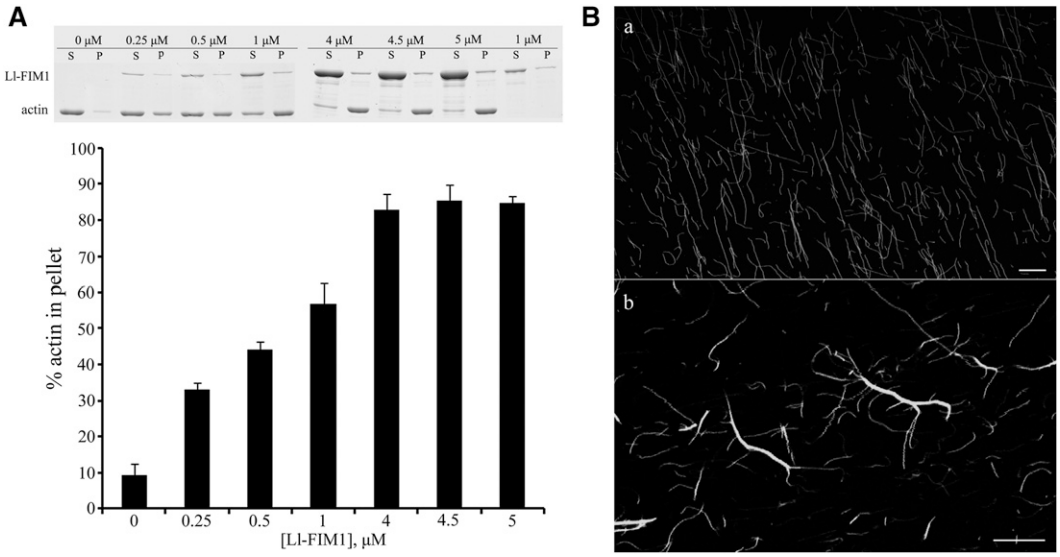

Figure 9. Ll-FIM1 Can Cross-Link F-Actin into Actin Bundles.

(A) Low-speed cosedimentation assays were used to determine the bundling activity of Ll-FIM1. Increasing concentrations of Ll-FIM1 (0.25 to 5 μM) were incubated with F-actin, and samples were subjected to low-speed cosedimentation assays. Gels were analyzed to determine the percentage of actin in the pellets. Error bars indicate mean ± SD (n = 3). P, pellet; S, supernatant.

(B) The ability of Ll-FIM1 to alter actin organization was visualized by Alexa-488 phalloidin staining of F-actin incubated in the absence (a) or presence of Ll-FIM1 (b). Bars = 10 μm.

proteins fragment actin bundles in the subapical area of pollen tubes when the Ca^{2+} concentration is increased and bundle actin filaments when the Ca^{2+} concentration is decreased. Moreover, P-135-ABP concentrates in the same area as the cortical actin fringe (Lovy-Wheeler et al., 2005), suggesting that P-135-ABP may function in actin fringe remodeling during the oscillatory growth of pollen tubes. The studies of *Arabidopsis* pollen-abundant PLIMs showed that PLIMs can bundle actin filaments only at low concentrations of H^+ (pH $\leq$ 6.8) because high pH values inhibit their bundling activities. Therefore, it is deducible that during the cyclic pH changes in oscillatory tip growth, the LIM protein transiently protects the short actin bundles of the cortical fringe when the alkaline band reaches its lowest pH values, down to 6.8. The research showing that the GFP-PLIM2c occasionally faintly labels a subapical structure resembling the actin cortical fringe (Papuga et al., 2010) provides some support for this speculation. However, it remains to be directly experimentally confirmed that villin and LIM proteins can stabilize the actin fringe in pollen tubes.

Fimbrin family proteins have long been known as ABPs that regulate the formation of higher-order actin filament structures. The reported plant fimbrins show some conserved biochemical characteristics, such as high affinity actin binding activity, actin filament bundling activity, etc. In vivo functional analysis of At-FIM1 shows that it stabilizes actin filaments against profilin-induced depolymerization (Kovar et al., 2000a). Similarly, it has been reported that At-FIM5 is required for the organization of actin filaments in pollen grains and pollen tubes (Wu et al., 2010). In this study, we find that Ll-FIM1 shares similar biochemical characteristics with its *Arabidopsis* homologs. In vitro biochemical analysis shows that the recombinant Ll-FIM1 protein has a high affinity for actin filaments, and unlike villin and LIM, Ll-FIM1 can organize actin filaments into bundles independently of Ca^{2+}. Moreover, our results show that the Ll-FIM1 protein performs bundling activities in both low and high pH conditions. We observed that the bundling activity of Ll-FIM1 was higher in pH 6.2 than in pH 7.4, indicating it may protect the cortical fringe during the cyclic pH changes in the oscillatory tip growth. In vivo, we found that the arrangement of the actin fringe was disturbed when the function of Ll-FIM1 was blocked by the injection of a specific anti-Ll-FIM1 antibody, which implies that Ll-FIM1 is involved in the organization of actin fringe. This is confirmed by a genetic complementation experiment in *fim5* mutants, the mutant of its closest relative in *Arabidopsis*. It has been reported that the loss of function of At-FIM5 resulted in a delay in pollen germination and curled morphology in pollen tube growth (Wu et al., 2010). We further discovered that during the early stage, in addition to the curled morphology, the diameters of *fim5* pollen tubes are wider than those of the wild type, but the morphological abnormalities could return to normal in the late stage. Of particular note, the subapical actin fringe is always impaired during tip growth of *fim5* mutants, and the stably expressed Ll-FIM1 can rescue the abnormal phenotype as well as the actin fringe structure in *fim5* mutants. Moreover, Ll-FIM1 obviously colocalizes with the subapical actin fringe in pollen tubes. Although Ll-FIM1 protein also localizes at actin bundles in the shank of pollen tubes, the actin architecture in the shank does not change significantly. Considering that cytoplasmic streaming is still occurring, we speculate that the decrease in velocity of cytoplasmic streaming may not be induced by the disturbance of the tracks in shank, but by the damage to the actin fringe in the subapical region, which induces disorder

in the apical region and thus slows down cytoplasmic streaming in the shank (Kroeger et al., 2009). Collectively, our results indicate that Ll-FIM1 may be responsible for the organization of the actin fringe through its actin bundling activity. It seems that villins and LIMs bundle actin cables in the shank of the pollen tube, where the Ca^{2+} concentration and pH are optimal for their bundling activities, but may periodically stabilize the actin bundles in the subapical/apical area. Therefore, it is possible that fimbrin is a key regulator in the formation of actin fringe.

The function of the actin fringe is somewhat more problematic. It has been shown that low concentrations of LatB have a profound but selective effect on the actin cytoskeleton of pollen tubes (i.e., it can destroy the cortical actin fringe but retain arrays of actin filaments in the shank of the tube) (Cárdenas et al., 2008). Corresponding to this phenomenon, elongation of pollen tubes is inhibited at much lower concentrations of actin drugs than those required to impede long-distance organelle movement (Gibbon et al., 1999; Vidali et al., 2001), indicating that the actin fringe in the subapex plays a central role in pollen tube growth. In our study, we observed that the anti-Ll-FIM1 antibody has the most profound influence on tip growth, a result similar to that induced by the application of a nanomolar level of LatB. Recent studies show that in growing pollen tubes, the front end or leading edge of the cortical actin fringe coincides with a region forming an annulus around the pole of the pollen tube tip, which is thought to correspond to the region of highest exocytosis (Bove et al., 2008; Bou Daher and Geitmann, 2011). Therefore, the cortical actin fringe may serve as a track to target cell wall vesicles to the exocytotic sites on the apical plasma membrane (Bove et al., 2008; Zonia and Munnik, 2008, 2009; Kroeger et al., 2009; Bou Daher and Geitmann, 2011). Our data demonstrate that the cortical actin fringe has only a close connection with growth rate but does not affect the polarity of the pollen tube. It is observed that there are still some short actin filaments in the subapical region of antibody-injected lily pollen tubes and *Arabidopsis fim5* mutant pollen tubes, which may fulfill part of the normal function of the actin fringe. It could be that the disruption of the short parallel actin bundles in the subapical region induces disordered exocytotic vesicle targeting and then inhibits the pollen tube growth.

To summarize, as an actin bundler, Ll-FIM1 plays a key role in the maintenance of the actin fringe, which is disturbed when the function of Ll-FIM1 is blocked. To support this, we demonstrated that stably expressing Ll-FIM1 in the *Arabidopsis fim5* pollen tube could rescue the actin fringe of the mutant. Our study provides a glimpse into the mechanism of actin fringe formation and shows that the *fim5* pollen tube is suitable for further exploration of actin fringe function in polar growth of pollen tubes.

METHODS

Plant Growth and Pollen Germination Conditions

Lily (*Lilium longiflorum*) was grown in the greenhouse, and 1- to 2-d-old anthers were collected for a fresh pollen source or placed at −80°C for later use. *Arabidopsis thaliana* T-DNA insertion lines, *fim5-1* (CS856909) with insertions in the *FIM5* gene, were obtained from the Nottingham Arabidopsis Stock Centre. *Arabidopsis* ecotype Col-0 was used as the wild-type plant (wild-type Col-0). All *Arabidopsis* lines were grown at 22°C in growth rooms under a light regime of 16 h light/8 h dark. *Arabidopsis* pollen grains were germinated on a solid germination medium (Boavida and McCormick, 2007) at 22°C under high humidity. Lily pollen grains were germinated in a liquid germination medium [10% Suc, 0.99 mM KNO_3, 0.08 mM $MgSO_4$, 0.162 mM H_3BO_3, and 1.27 mM $Ca(NO_3)_2$, pH 5.6] at 28°C, 100 rpm.

Full-Length cDNA Cloning and Expression Profile Analysis of Ll-*FIM1*

A partial sequence of cDNA of *FIM1* was obtained from a lily pollen expression cDNA library (kindly provided by Peter K. Hepler, University of Massachusetts, Amherst, MA). The full-length sequence of cDNA of *FIM1* was obtained from first-strand cDNA synthesized from lily pollen total RNA and 5′-rapid amplification of cDNA ends according to the manufacturer's protocol (SMART RACE cDNA amplification kit; Clontech). RT-PCR analysis was performed with a gene-specific primer set: RTLl-FIM1-S and RTLl-FIM1-A. To monitor the efficiency of cDNA synthesis by PCR amplification, the housekeeping gene *ACTlN* was used as an internal control for PCR amplification, obtained using a specific primer set: Ll-Actin-S and Ll-Actin-A. Primer sequences are listed in Supplemental Table 1 online.

Plasmid Construction

To complement *Arabidopsis fim5* mutants, an N-terminal fusion of Ll-FIM1 with GFP was constructed by PCR-based methodology, introducing an *Xba*I site at the 5′ end of the GFP coding region and a *Kpn*I site at the 3′ end of the Ll-FIM1 coding region using the primers GFP-S and GFP-A (for GFP amplification), and Ll-FIM1-S and Ll-FIM1ORF-A (for Ll-FIM1 amplification). The GFP-At-FIM5 segment was obtained similarly using the primers GFP-S and GFP-A (for GFP amplification), and At-FIM5-S and At-FIM5ORF-A (for At-FIM5 amplification). The *Xba*I-*Kpn*I or *Xba*I-*Sma*II fragment was then cloned into pCAMBIA1300. The At-FIM5 promoter (including 1090 bp upstream of the start codon) was amplified using the At-fim5p-S and At-fim5p-A primers, and then the 35S promoter was subsequently replaced by digesting the *Sph*I or *Sal*I and *Xba*I sites to construct the binary vector pCAMBIA1300-fim5p-GFP-Ll-FIM1 and pCAMBIA1300-fim5p-GFP-At-FIM5. The plasmids used for overexpressing Ll-FIM1 recombinant protein in *Escherichia coli* for antibody production were derived from pGEX-6P-1 vector. The C-terminal sequence of Ll-FIM1 (620-690AA) was amplified using Ll-FIM1antibody-S and Ll-FIM1antibody-A primers, and then the *Sal*I-*Not*I fragment was then subcloned into pGEX-6P-1 (Amersham) and confirmed by sequencing. The plasmids used for overexpressing 6×His-tagged recombinant protein in *E. coli* were derived from pET-30a (+) vector (Novagen). The coding sequence for Ll-FIM1 was amplified using Ll-FIM1ORF-S and Ll-FIM1ORF-A primers, and then the *Sal*I-*Kpn*I fragment was then subcloned into pET-30a(+) and confirmed by sequencing.

Expression and Purification of Recombinant At-FIM5, Ll-FIM1, and Ll-FIM1 Antigen

For recombinant At-FIM5 and Ll-FIM1, the constructs were transformed into strain BL21 (DE3) of *E. coli.* The cells were grown at 37°C for 3 h and then induced by the addition of 0.4 mM isopropyl-D-thiogalactopyranoside at 22°C overnight. Cells were collected by centrifugation and resuspended in binding buffer (400 mM NaCl and 40 mM PBS, pH 8.0) supplemented with 0.5 mM phenylmethylsulfonyl fluoride (PMSF). This was followed by purification using nickel-nitrilotriacetic acid (Ni-NTA) His bind resin following the protocol in the manufacturer's manual (Novagen). The purified proteins were dialyzed overnight against buffer TK (5 mM Tris-HCl, 50 mM KCl, 0.5 mM EDTA, and 0.5 mM DTT, pH 7.5) and stored in aliquots in liquid nitrogen. To obtain the Ll-FIM1 antigen, cells were collected by centrifugation and resuspended in PBS (137 mM NaCl, 2.7 mM KCl, 10 mM Na_2HPO_4, and 2 mM KH_2PO_4, pH 8.0) supplemented with 0.5 mM PMSF. This was followed by purification using

a glutathione–Sepharose 4B resin following the protocol in the manufacturer's manual (Novagen). The purified protein was dialyzed overnight against PBS. Protein concentrations were determined with the Bradford reagent (Bio-Rad) using BSA as a standard.

Cosedimentation Assays

High-speed cosedimentation assays were performed as described previously (Kovar et al., 2000b). Briefly, 3.0 μM G-actin was incubated in 1× F buffer (10× stock: 50 mM Tris-Cl, pH 7.5, 5 mM DTT, 5 mM ATP, 1 M KCl, and 50 mM $MgCl_2$) in the presence of 2.0 mM EGTA (added from a 200 mM stock in 1× F buffer). The final concentration of free calcium, [Ca^{2+}], was 40 nM as computed with the MAXC programs (available at http://www.stanford.edu/~cpatton/maxc.html). Then, in a 200 μL reaction volume, either 3.0 μM preassembled actin alone, 1.0 μM LI-FIM1 alone, or preassembled actin with LI-FIM1 were incubated for 60 min at 22°C. Following incubation, 80 μL of the reaction mix (total sample) was transferred to another tube with 20 μL of 5× SDS-PAGE sample buffer. The remaining mix was centrifuged for 30 min at 200,000*g* at 4°C, and the supernatants and pellets were resolved on SDS-PAGE gels and stained with Coomassie Brilliant Blue. The intensities of the resulting bands were quantified by densitometry using QuantityOne v4.6.5 software (Bio-Rad). The apparent dissociation constant (K_d) value was determined according to the method of Khurana et al. (2010). Briefly, Increasing amounts of actin (0.5, 0.75, 1.0, 1.5, 2.0, 3.0, 4.0, and 6.0 μM) were incubated with 0.8 μM LI-FIM1 for 60 min at 22°C followed by a 30-min spin at 200,000*g*. The free Ca^{2+} concentration was 40 nM in these reactions. The percentage of bound protein as a function of actin concentration was plotted and fitted to a hyperbolic function using Kaleidagraph software (Synergy Software).

Low-speed cosedimentation assays were performed according the methods of Thomas et al. (2006). Briefly, increasing amounts of LI-FIM1 (0.25 to 5 μM) were incubated with 3 μM preassembled F-actin for 1 h at 22°C. Samples were centrifuged at 13,500*g* for 30 min in a microcentrifuge at 4°C and analyzed by SDS-PAGE as previously described. After quantification, results were expressed as percentage of actin in the pellet in function of LI-FIM1 concentration.

The effect of Ca^{2+} on bundling activity was examined by incubating 1 μM LI-FIM1 with 3 μM F-actin and various concentrations of free Ca^{2+} (0.01 to 100 μM). The effect of pH on bundling activity was examined as described previously (Papuga et al., 2010) with some modifications. Briefly, actin was copolymerized with various concentrations of LI-FIM1 for 1 h in the presence of 1× KMEI (50 mM KCl, 1 mM $MgCl_2$, 1 mM EGTA, and 10 mM imidazole). The reaction medium was composed of PIPES and Tris that was adjusted to pH 6.2 or 7.4.

Visualization of Actin Filament Cross-Linking by Fluorescence Microscopy

F-actin (3.0 μM) was incubated with 1 μM LI-FIM1 in the presence of 200 μM Ca^{2+} for 60 min at room temperature and labeled with an equimolar amount of Alexa-488 phalloidin (Molecular Probes). F-actin was diluted to 50 nM with 1× F buffer, and 2 μL of the diluted sample was added to a 22 × 22-mm cover slip coated with poly-Lys (0.01%) before observation. Actin filaments for static observation were viewed using a confocal laser scanning microscope (Olympus FV-300) mounted on an inverted microscope (Olympus IX-70) with a ×60 oil immersion objective, and the images were collected by Olympus Fluoview 4.0 software.

Protein Extraction and Immunoblotting

Pollen proteins were extracted by homogenization in buffer (0.1 M Tris-HCl, 0.5 M $CaCl_2$, 0.05 M NaF, 0.4 M D-Sorbitol, 0.5 mM ATP, 5 mM DTT, and 0.5 mM PMSF, pH 7.0) and analyzed using SDS-PAGE. After SDS-PAGE, proteins on the 12% polyacrylamide gel were electrophoretically transferred to a polyvinylidene difluoride membrane (Millipore) according to the method of Towbin et al. (1992), and the blot was blocked with PBS containing 5% BSA and 0.1% Tween 20 for 90 min. Purified LI-FIM1 polyclonal antibody was diluted 1000-fold with PBS supplemented with 3% BSA and 0.1% Tween 20. Anti-rabbit IgG conjugated with alkaline phosphatase was diluted 2000-fold as secondary antibody.

Fixation and Immunolocalization

Lily pollen tubes were cultured for 1 to 2 h and simultaneously fixed and permeabilized with 4% formaldehyde and 0.5% glutaraldehyde in PEM buffer (50 mM PIPES, 5 mM $MgSO_4$, 5 mM EGTA, and 0.1 M mannitol, pH 6.9) under vacuum for 40 min. The fixative was removed, and the cells were washed three times with PEM buffer and then incubated in 0.5% cellulase/0.25% pectinase for 20 min at 30°C. After washing, cells were treated with 1 mg/mL $NaBH_4$ in PBS for 15 min and then incubated in blocking solution (1% BSA in PBS) for 30 min at room temperature. Pollen tubes were incubated with primary antibody 1:100 diluted in blocking solution overnight at 4°C. Following PBS washes, pollen tubes were incubated with the secondary antibody for 1.5 h at room temperature followed by further PBS washes. F-actin was stained using 200 nM Alexa-568 phalloidin (Invitrogen).

For LatB treatment, stock solutions of LatB were dissolved in DMSO, and working stocks were made fresh by further dilution in liquid germination medium. After treatment for 1 min, the pollen tubes then immediately fixed.

Rapid freeze fixation and immunolabeling experiments were performed as described previously (Lovy-Wheeler et al., 2005). A monoclonal mouse antiactin antibody (raised against *Arabidopsis* ACT11 full-length protein; AbMART) was applied.

Microinjection Procedures

Microinjection experiments were performed as described previously (Lin and Yang, 1997). Approximately 1 h after germination, pollen tubes ~250 μm in length were chosen for injection. Approximately 0.3 nL of agents was injected into each pollen tube. The affinity-purified antibody was gently loaded into the pollen cytoplasm, and 5 min after injection, micropipette tips were slowly removed from the pollen tube, followed by time-lapse recording of the subsequent growth of pollen tubes. BSA (0.5 mg/mL) in the buffer (5 mM Tris-HCl, pH 7.0) and the buffer alone served as the controls. For observation of actin filaments after injection, the pollen tubes were simultaneously fixed as described previously (Lovy-Wheeler et al., 2005).

Aniline Blue Staining Assay

Preemasculated mature wild-type flowers were pollinated either with wild-type or *fim5-1* pollen. After 8 to 12 h, the pollinated pistils were fixed in fixing solution containing ethanol:acetic acid (3:1) for 2 h at room temperature, washed with distilled water three times for 5 min each, and then the pistils were incubated in 8 M NaOH softening solution overnight. The following day, the pistils were washed in distilled water three times for 1 h each. The pistils were then stained in aniline blue solution (0.1% aniline blue in 0.1 M K_2HPO_4-KOH buffer, pH 11) for 5 h in the absence of light and were observed with Leica DFC 425C digital camera on Leica M165FC stereozoom microscope (Leica Microsystems).

Labeling of Actin Filaments in *Arabidopsis* Pollen Tubes

To visualize the actin cytoskeleton in *Arabidopsis* pollen tubes, pollen was fixed as described previously (Zhang et al., 2011), with some modifications. Pollen tubes were prefixed for 2 min with 100 μM *m*-maleimidobenzoyl *N*-hydroxysuccinimide ester (Sigma-Aldrich) in 1% freshly prepared

formaldehyde and 0.025% glutaraldehyde in actin-stabilizing buffer (ASB; 50 mM PIPES, 0.5 mM $MgCl_2$, 0.5 mM $CaCl_2$, and 37 mM KCl, pH 6.8). This was followed by immersion in 200 μM ester, 2% formaldehyde, and 0.05% glutaraldehyde in ASB for 20 min. Pollen tubes were then fixed in a final concentration of 4% formaldehyde and 0.1% glutaraldehyde in ASB for 20 min, followed by permeabilization with 0.02% Nonidet P-40 in ASB for 30 min, and the actin cytoskeleton was stained with 200 nM Alexa-488/Alexa-568 phalloidin (Molecular Probes) in the same buffer. Actin filaments were visualized using a confocal laser scanning microscope (Olympus FV-300) mounted on an inverted microscope (Olympus IX-70). Serial confocal optical sections were taken at a step size of 0.5 μm using Olympus Fluoview 4.0 software.

Quantitative Analysis of Actin Filament Bundling and Density in Pollen Tubes

To quantify the extent of bundling and actin abundance in tip and shank areas of antibody-injected lily pollen tubes and *Arabidopsis* pollen tubes, a skewness and density analysis was performed according to the method described (Higaki et al., 2010; Henty et al., 2011). For the tip measurements, we selected a fixed region (13 μm in length and 19 μm in width for lily pollen tubes and 12 μm in length and 10 μm in width for *Arabidopsis* pollen tubes) in the tip of pollen tube for skewness and density analysis. For the shank measurements, we selected a fixed region (55 μm in length and 20 μm in width for lily pollen tubes and 30 μm [the early stage] or 60 μm [the late stage] in length and 10 μm in width for *Arabidopsis* pollen tubes), which was 20 μm (for lily pollen tubes) or 10 μm (for *Arabidopsis* pollen tubes) from the tip of the pollen tube, for skewness and density analysis.

For the skewness analysis, the z-series stacks of all optical sections were filtered using Gaussian blur to reduce background noise and then skeletonized using the procedure of ThinLine (a JAVA plug-in procedure; see Higaki et al., 2010). The actin filament pixels were collected into a single image using maximum-intensity projections, and the skewness values were calculated.

For the density analysis, the z-series stacks of all optical sections were filtered using Gaussian blur to reduce background noise, and then the actin filament pixels were collected into a single image using maximum-intensity projections. After high band-pass filtering, image threshold settings were set to include all actin filaments, images were converted to binary black and white, and then the occupancy values were calculated.

Quantitative Colocalization of F-Actin and Ll-FIM1

To quantify the extent of the colocalization of Ll-FIM1 with the actin filaments, the PSC colocalization plug-in (French et al., 2008) for ImageJ was used to calculate r_p and r_s of red and green fluorescent signals. Values were between −1 (negative correlation) and +1 (positive correlation). For the lily pollen tubes, a fixed region (15 μm in length and 18 μm in width) in the tip and shank area were selected and analyzed. For the *Arabidopsis* pollen tubes, a fixed region (12 μm in length and 10 μm in width) in the tip was selected and analyzed.

To verify further the colocalization of Ll-FIM1 with the actin filaments in lily pollen tubes and the colocalization of GFP-Ll-FIM1 with the actin fringe in *Arabidopsis* pollen tubes, we applied a method according to Poulter et al. (2010). Briefly, colocalization quantification was performed using MetaMorph software (Molecular Devices) on the projection (for lily pollen tubes) or middle optical sections (for *Arabidopsis* pollen tubes) obtained by laser scanning confocal microscopy. For measuring the average level of background fluorescence for all images, 10 boxes were placed throughout a region corresponding to the shank/tip area of the lily pollen tube or the tip of the *Arabidopsis* pollen tube; for measuring the extent of colocalization, five to 15 boxes were selected.

Accession Numbers

Sequence data from this article can be found in the Arabidopsis Genome Initiative or GenBank/EMBL databases under the following accession numbers: Ll-FIM1 (lily fimbrin1, JX910418), At-FIM5 (*Arabidopsis* FIMBRIN5, NP_198420; At5g35700), Sac6p (*Saccharomyces cerevisiae*, NP_010414), and T-plastin (*Homo sapiens*, NP_005023).

Supplemental Data

The following materials are available in the online version of this article.

Supplemental Figure 1. Alignment of Amino Acid Sequence of Ll-FIM1 with Fimbrin Family Members from *Arabidopsis*, Yeast, and Human.

Supplemental Figure 2. Phylogenetic Analysis of Ll-FIM1 with Fimbrin-Like Proteins from *Arabidopsis*, Rice, Maize, Moss, Yeast, and Human.

Supplemental Figure 3. FIM1 Colocalized with the Actin Fringe in *L. longiflorum* Pollen Tubes.

Supplemental Figure 4. Velocity of Cytoplasmic Streaming Was Significantly Reduced in the Shank Area of Antibody-Injected Lily Pollen Tubes.

Supplemental Figure 5. Effects of Antibody Injection on the Organization of Actin Filaments in Lily Pollen Tubes.

Supplemental Figure 6. The Pollen Tube Elongation Rate Was Recovered in GFP-Ll-FIM1 Complemented Lines.

Supplemental Figure 7. GFP-Ll-FIM1 Protein Concentrated at the Subapical Actin Fringe in Complemented Pollen Tubes.

Supplemental Figure 8. Localization of GFP-Ll-FIM1 in Growing Pollen Tubes.

Supplemental Figure 9. Ll-FIM1 Bundles Actin Filaments in a Ca^{2+}-Independent Manner.

Supplemental Figure 10. The Effect of pH on Bundling Activity of Ll-FIM1 Was Determined by Low-Speed Cosedimentation Assays at pH 6.2 and pH 7.4.

Supplemental Table 1. Nucleotide Sequences of Primer Sets Used in This Study.

Supplemental Data Set 1. Text File of the Alignment Used to Generate the Phylogenetic Tree in Supplemental Figure 2.

ACKNOWLEDGMENTS

We thank Peter K. Hepler (University of Massachusetts, Amherst, MA) for kindly providing the lily pollen cDNA expression Library. This work was supported by the National Natural Science Foundation of China (31130005) and by the National Basic Research Program of China (2013CB126902) to H.R.

AUTHOR CONTRIBUTIONS

H.R. and H.S. designed the research, wrote the article, and analyzed the data. H.S., J.Z., and C.C. performed most of the experiments. W.P., J.W., and H.D. performed some experiments.

Received April 10, 2012; revised September 29, 2012; accepted October 17, 2012; published November 13, 2012.

REFERENCES

Allwood, E.G., Anthony, R.G., Smertenko, A.P., Reichelt, S., Drobak, B.K., Doonan, J.H., Weeds, A.G., and Hussey, P.J. (2002). Regulation of the pollen-specific actin-depolymerizing factor LlADF1. Plant Cell **14:** 2915–2927.

Boavida, L.C., and McCormick, S. (2007). Temperature as a determinant factor for increased and reproducible *in vitro* pollen germination in *Arabidopsis thaliana*. Plant J. **52:** 570–582.

Bou Daher, F., and Geitmann, A. (2011). Actin is involved in pollen tube tropism through redefining the spatial targeting of secretory vesicles. Traffic **12:** 1537–1551.

Bove, J., Vaillancourt, B., Kroeger, J., Hepler, P.K., Wiseman, P.W., and Geitmann, A. (2008). Magnitude and direction of vesicle dynamics in growing pollen tubes using spatiotemporal image correlation spectroscopy and fluorescence recovery after photobleaching. Plant Physiol. **147:** 1646–1658.

Cai, G., and Cresti, M. (2009). Organelle motility in the pollen tube: A tale of 20 years. J. Exp. Bot. **60:** 495–508.

Cárdenas, L., Lovy-Wheeler, A., Kunkel, J.G., and Hepler, P.K. (2008). Pollen tube growth oscillations and intracellular calcium levels are reversibly modulated by actin polymerization. Plant Physiol. **146:** 1611–1621.

Chen, C.Y., Wong, E.I., Vidali, L., Estavillo, A., Hepler, P.K., Wu, H.M., and Cheung, A.Y. (2002). The regulation of actin organization by actin-depolymerizing factor in elongating pollen tubes. Plant Cell **14:** 2175–2190.

Chen, N., Qu, X., Wu, Y., and Huang, S. (2009). Regulation of actin dynamics in pollen tubes: Control of actin polymer level. J. Integr. Plant Biol. **51:** 740–750.

Cheung, A.Y., Niroomand, S., Zou, Y., and Wu, H.M. (2010). A transmembrane formin nucleates subapical actin assembly and controls tip-focused growth in pollen tubes. Proc. Natl. Acad. Sci. USA **107:** 16390–16395.

Cheung, A.Y., and Wu, H.M. (2008). Structural and signaling networks for the polar cell growth machinery in pollen tubes. Annu. Rev. Plant Biol. **59:** 547–572.

Cole, R.A., and Fowler, J.E. (2006). Polarized growth: Maintaining focus on the tip. Curr. Opin. Plant Biol. **9:** 579–588.

Fan, X., Hou, J., Chen, X., Chaudhry, F., Staiger, C.J., and Ren, H. (2004). Identification and characterization of a Ca^{2+}-dependent actin filament-severing protein from lily pollen. Plant Physiol. **136:** 3979–3989.

Feijó, J.A., Sainhas, J., Hackett, G.R., Kunkel, J.G., and Hepler, P.K. (1999). Growing pollen tubes possess a constitutive alkaline band in the clear zone and a growth-dependent acidic tip. J. Cell Biol. **144:** 483–496.

Franklin-Tong, V.E. (1999). Signaling and the modulation of pollen tube growth. Plant Cell **11:** 727–738.

French, A.P., Mills, S., Swarup, R., Bennett, M.J., and Pridmore, T.P. (2008). Colocalization of fluorescent markers in confocal microscope images of plant cells. Nat. Protoc. **3:** 619–628.

Fu, Y. (2010). The actin cytoskeleton and signaling network during pollen tube tip growth. J. Integr. Plant Biol. **52:** 131–137.

Fu, Y., Wu, G., and Yang, Z. (2001). Rop GTPase-dependent dynamics of tip-localized F-actin controls tip growth in pollen tubes. J. Cell Biol. **152:** 1019–1032.

Geitmann, A., Snowman, B.N., Emons, A.M., and Franklin-Tong, V.E. (2000). Alterations in the actin cytoskeleton of pollen tubes are induced by the self-incompatibility reaction in *Papaver rhoeas*. Plant Cell **12:** 1239–1251.

Gibbon, B.C., Kovar, D.R., and Staiger, C.J. (1999). Latrunculin B has different effects on pollen germination and tube growth. Plant Cell **11:** 2349–2363.

Henty, J.L., Bledsoe, S.W., Khurana, P., Meagher, R.B., Day, B., Blanchoin, L., and Staiger, C.J. (2011). *Arabidopsis* actin depolymerizing factor4 modulates the stochastic dynamic behavior of actin filaments in the cortical array of epidermal cells. Plant Cell **23:** 3711–3726.

Higaki, T., Kutsuna, N., Sano, T., Kondo, N., and Hasezawa, S. (2010). Quantification and cluster analysis of actin cytoskeletal structures in plant cells: role of actin bundling in stomatal movement during diurnal cycles in *Arabidopsis* guard cells. Plant J. **61:** 156–165.

Huang, S., Blanchoin, L., Chaudhry, F., Franklin-Tong, V.E., and Staiger, C.J. (2004). A gelsolin-like protein from *Papaver rhoeas* pollen (PrABP80) stimulates calcium-regulated severing and depolymerization of actin filaments. J. Biol. Chem. **279:** 23364–23375.

Khurana, P., Henty, J.L., Huang, S., Staiger, A.M., Blanchoin, L., and Staiger, C.J. (2010). *Arabidopsis* VILLIN1 and VILLIN3 have overlapping and distinct activities in actin bundle formation and turnover. Plant Cell **22:** 2727–2748.

Klein, M.G., Shi, W., Ramagopal, U., Tseng, Y., Wirtz, D., Kovar, D.R., Staiger, C.J., and Almo, S.C. (2004). Structure of the actin crosslinking core of fimbrin. Structure **12:** 999–1013.

Kost, B., Spielhofer, P., and Chua, N.H. (1998). A GFP-mouse talin fusion protein labels plant actin filaments *in vivo* and visualizes the actin cytoskeleton in growing pollen tubes. Plant J. **16:** 393–401.

Kovar, D.R., Drøbak, B.K., and Staiger, C.J. (2000a). Maize profilin isoforms are functionally distinct. Plant Cell **12:** 583–598.

Kovar, D.R., Staiger, C.J., Weaver, E.A., and McCurdy, D.W. (2000b). AtFim1 is an actin filament crosslinking protein from *Arabidopsis thaliana*. Plant J. **24:** 625–636.

Kroeger, J.H., Daher, F.B., Grant, M., and Geitmann, A. (2009). Microfilament orientation constrains vesicle flow and spatial distribution in growing pollen tubes. Biophys. J. **97:** 1822–1831.

Lee, Y.J., Szumlanski, A., Nielsen, E., and Yang, Z. (2008). Rho-GTPase-dependent filamentous actin dynamics coordinate vesicle targeting and exocytosis during tip growth. J. Cell Biol. **181:** 1155–1168.

Lenartowska, M., and Michalska, A. (2008). Actin filament organization and polarity in pollen tubes revealed by myosin II subfragment 1 decoration. Planta **228:** 891–896.

Lin, Y., and Yang, Z. (1997). Inhibition of pollen tube elongation by microinjected anti-Rop1Ps antibodies suggests a crucial role for Rho-Type GTPases in the control of tip growth. Plant Cell **9:** 1647–1659.

Lovy-Wheeler, A., Kunkel, J.G., Allwood, E.G., Hussey, P.J., and Hepler, P.K. (2006). Oscillatory increases in alkalinity anticipate growth and may regulate actin dynamics in pollen tubes of lily. Plant Cell **18:** 2182–2193.

Lovy-Wheeler, A., Wilsen, K.L., Baskin, T.I., and Hepler, P.K. (2005). Enhanced fixation reveals the apical cortical fringe of actin filaments as a consistent feature of the pollen tube. Planta **221:** 95–104.

Nakayasu, T., Yokota, E., and Shimmen, T. (1998). Purification of an actin-binding protein composed of 115-kDa polypeptide from pollen tubes of lily. Biochem. Biophys. Res. Commun. **249:** 61–65.

Papuga, J., Hoffmann, C., Dieterle, M., Moes, D., Moreau, F., Tholl, S., Steinmetz, A., and Thomas, C. (2010). *Arabidopsis* LIM proteins: A family of actin bundlers with distinct expression patterns and modes of regulation. Plant Cell **22:** 3034–3052.

Pierson, E.S., Miller, D.D., Callaham, D.A., Shipley, A.M., Rivers, B.A., Cresti, M., and Hepler, P.K. (1994). Pollen tube growth is coupled to the extracellular calcium ion flux and the intracellular calcium gradient: Effect of BAPTA-type buffers and hypertonic media. Plant Cell **6:** 1815–1828.

Poulter, N.S., Staiger, C.J., Rappoport, J.Z., and Franklin-Tong, V.E. (2010). Actin-binding proteins implicated in the formation of the punctate actin foci stimulated by the self-incompatibility response in *Papaver*. Plant Physiol. **152:** 1274–1283.

Rathore, K.S., Cork, R.J., and Robinson, K.R. (1991). A cytoplasmic gradient of Ca2+ is correlated with the growth of lily pollen tubes. Dev. Biol. **148:** 612–619.

Ren, H., and Xiang, Y. (2007). The function of actin-binding proteins in pollen tube growth. Protoplasma **230:** 171–182.

Snowman, B.N., Kovar, D.R., Shevchenko, G., Franklin-Tong, V.E., and Staiger, C.J. (2002). Signal-mediated depolymerization of actin in pollen during the self-incompatibility response. Plant Cell **14:** 2613–2626.

Staiger, C.J., Poulter, N.S., Henty, J.L., Franklin-Tong, V.E., and Blanchoin, L. (2010). Regulation of actin dynamics by actin-binding proteins in pollen. J. Exp. Bot. **61:** 1969–1986.

Thomas, C., Hoffmann, C., Dieterle, M., Van Troys, M., Ampe, C., and Steinmetz, A. (2006). Tobacco WLIM1 is a novel F-actin binding protein involved in actin cytoskeleton remodeling. Plant Cell **18:** 2194–2206.

Thomas, C., Tholl, S., Moes, D., Dieterle, M., Papuga, J., Moreau, F., and Steinmetz, A. (2009). Actin bundling in plants. Cell Motil. Cytoskeleton **66:** 940–957.

Tominaga, M., Yokota, E., Vidali, L., Sonobe, S., Hepler, P.K., and Shimmen, T. (2000). The role of plant villin in the organization of the actin cytoskeleton, cytoplasmic streaming and the architecture of the transvacuolar strand in root hair cells of *Hydrocharis*. Planta **210:** 836–843.

Towbin, H., Staehelin, T., and Gordon, J. (1992). Electrophoretic transfer of proteins from polyacrylamide gels to nitrocellulose sheets: Procedure and some applications. 1979. Biotechnology **24:** 145–149.

Vidali, L., and Hepler, P.K. (1997). Characterization and localization of profilin in pollen grains and tubes of *Lilium longiflorum*. Cell Motil. Cytoskeleton **36:** 323–338.

Vidali, L., McKenna, S.T., and Hepler, P.K. (2001). Actin polymerization is essential for pollen tube growth. Mol. Biol. Cell **12:** 2534–2545.

Vidali, L., Rounds, C.M., Hepler, P.K., and Bezanilla, M. (2009). Lifeact-mEGFP reveals a dynamic apical F-actin network in tip growing plant cells. PLoS ONE **4:** e5744.

Wang, H.J., Wan, A.R., and Jauh, G.Y. (2008). An actin-binding protein, LILIM1, mediates calcium and hydrogen regulation of actin dynamics in pollen tubes. Plant Physiol. **147:** 1619–1636.

Wu, Y., Yan, J., Zhang, R., Qu, X., Ren, S., Chen, N., and Huang, S. (2010). *Arabidopsis* FIMBRIN5, an actin bundling factor, is required for pollen germination and pollen tube growth. Plant Cell **22:** 3745–3763.

Xiang, Y., Huang, X., Wang, T., Zhang, Y., Liu, Q., Hussey, P.J., and Ren, H. (2007). ACTIN BINDING PROTEIN 29 from *Lilium* pollen plays an important role in dynamic actin remodeling. Plant Cell **19:** 1930–1946.

Ye, J., Zheng, Y., Yan, A., Chen, N., Wang, Z., Huang, S., and Yang, Z. (2009). *Arabidopsis* formin3 directs the formation of actin cables and polarized growth in pollen tubes. Plant Cell **21:** 3868–3884.

Yokota, E., Muto, S., and Shimmen, T. (2000). Calcium-calmodulin suppresses the filamentous actin-binding activity of a 135-kilodalton actin-bundling protein isolated from lily pollen tubes. Plant Physiol. **123:** 645–654.

Yokota, E., Takahara, K., and Shimmen, T. (1998). Actin-bundling protein isolated from pollen tubes of lily. Biochemical and immunocytochemical characterization. Plant Physiol. **116:** 1421–1429.

Yokota, E., Tominaga, M., Mabuchi, I., Tsuji, Y., Staiger, C.J., Oiwa, K., and Shimmen, T. (2005). Plant villin, lily P-135-ABP, possesses G-actin binding activity and accelerates the polymerization and depolymerization of actin in a Ca^{2+}-sensitive manner. Plant Cell Physiol. **46:** 1690–1703.

Yokota, E., Vidali, L., Tominaga, M., Tahara, H., Orii, H., Morizane, Y., Hepler, P.K., and Shimmen, T. (2003). Plant 115-kDa actin-filament bundling protein, P-115-ABP, is a homologue of plant villin and is widely distributed in cells. Plant Cell Physiol. **44:** 1088–1099.

Zhang, H., Qu, X., Bao, C., Khurana, P., Wang, Q., Xie, Y., Zheng, Y., Chen, N., Blanchoin, L., Staiger, C.J., and Huang, S. (2010). *Arabidopsis* VILLIN5, an actin filament bundling and severing protein, is necessary for normal pollen tube growth. Plant Cell **22:** 2749–2767.

Zhang, Y., Xiao, Y.Y., Du, F., Cao, L.J., Dong, H.J., and Ren, H. (2011). *Arabidopsis* VILLIN4 is involved in root hair growth through regulating actin organization in a Ca^{2+}-dependent manner. New Phytol. **190:** 667–682.

Zonia, L. (2010). Spatial and temporal integration of signalling networks regulating pollen tube growth. J. Exp. Bot. **61:** 1939–1957.

Zonia, L., and Munnik, T. (2008). Vesicle trafficking dynamics and visualization of zones of exocytosis and endocytosis in tobacco pollen tubes. J. Exp. Bot. **59:** 861–873.

Zonia, L., and Munnik, T. (2009). Uncovering hidden treasures in pollen tube growth mechanics. Trends Plant Sci. **14:** 318–327.